

Error Analysis of Tissue Resistivity Measurement

Jang-Zern Tsai, James A. Will, Scott Hubbard-Van Stelle, Hong Cao, *Student Member, IEEE*,
 Supan Tungjitkusolmun, *Member, IEEE*, Young Bin Choy, *Student Member, IEEE*,
 Dieter Haemmerich, *Student Member, IEEE*, Vicken R. Vorperian, and John G. Webster*, *Life Fellow, IEEE*

Abstract—We identified the error sources in a system for measuring tissue resistivity at eight frequencies from 1 Hz to 1 MHz using the four-terminal method. We expressed the measured resistivity with an analytical formula containing all error terms. We conducted practical error measurements with *in-vivo* and bench-top experiments. We averaged errors at all frequencies for all measurements. The standard deviations of error of the quantization error of the 8-bit digital oscilloscope with voltage averaging, the nonideality of the circuit, the *in-vivo* motion artifact and electrical interference combined to yield an error of $\pm 1.19\%$. The dimension error in measuring the syringe tube for measuring the reference saline resistivity added $\pm 1.32\%$ error. The estimation of the working probe constant by interpolating a set of probe constants measured in reference saline solutions added $\pm 0.48\%$ error. The difference in the current magnitudes used during the probe calibration and that during the tissue resistivity measurement caused $\pm 0.14\%$ error. Variation of the electrode spacing, alignment, and electrode surface property due to the insertion of electrodes into the tissue caused $\pm 0.61\%$ error. We combined the above errors to yield an overall standard deviation error of the measured tissue resistivity of $\pm 1.96\%$.

Index Terms—Calibration, electrode, error analysis, error measurement, four terminals, noise measurement, probe constant, tissue resistivity.

I. INTRODUCTION

RESEARCHERS have used various methods to measure tissue resistivity. Among them, the four-terminal technique has become the most popular because of its ability to minimize the error caused by the electrode-tissue interface impedance in the measured resistivity. Normally, with the four-terminal method, a resistivity probe comprises two current electrodes for delivering and collecting the current flowing through the tissue and two voltage electrodes between the

two current electrodes for sensing the voltage drop due to the current flow through the tissue. The tissue resistivity is calculated as

$$\rho = R_a \times K_p \quad (1)$$

where R_a , the apparent resistance, is the ratio of the voltage difference sensed by the two voltage electrodes and the current delivered and collected by the two current electrodes and K_p , the probe constant, is the ratio of the tissue resistivity divided by the apparent resistance. The probe constant is determined by the electrode configuration of the resistivity probe and is measured by calibration with a reference material.

Due to the differences in the purpose of measurement, accuracy requirement, animal species, tissue types, and the availability of instruments for resistivity measurement systems, there have been variations of the resistivity probe design, the instrumentation, and how the measurement is conducted.

Van Oosterom *et al.* [1] measured the intramural resistivity of canine hearts *in-vivo* from 10 Hz to 5 kHz using a four-terminal configuration with four consecutive electrodes of the 20 0.05 mm^2 electrode contacts along a shaft. They detected the voltage difference between the voltage electrodes with a differential amplifier and then utilized the phase of the current source to control the operation of two sample and hold circuits to detect the phase difference between the voltage and the current with another differential amplifier. Zheng *et al.* [2] measured the excised skeletal muscle resistivity of five mammals and chickens from 1 Hz to 1 MHz with a four-electrode cylindrical Plexiglas tube. They detected voltage difference between the two inner electrodes with a differential amplifier and the current through the muscle with a current-to-voltage converter and measured the output of the circuits with analog oscilloscopes. Ackmann [3] designed a four-terminal system for measuring complex bioelectric impedance from 5 Hz to 100 kHz with a Princeton Applied Research (PAR) Model 5404 lock-in amplifier and from 100 kHz to 1 MHz with a PAR Model 5402 lock-in amplifier. In his configuration, the amplitude and phase of the voltage difference between the two voltage electrodes were measured with a phase-sensitive detection technique using a signal in phase with the current as the reference. Steendijk *et al.* [4] measured canine myocardial resistivity *in-vivo* with a resistivity probe embedded in a suction cup, which attached the resistivity probe onto the epicardial surface. The resistivity probe had two perpendicular arrays of four point surface electrodes. They measured the myocardial resistivity from 5 kHz to 60 kHz with a modified analog-signal conditioner-processor (Leycom Sigma-5, CardioDynamics, Rijnsburg, The Netherlands), which was originally developed for intraventricular volume-conduc-

Manuscript received June 10, 2001; revised January 21, 2001. This work was supported by the National Institutes of Health (NIH) under Grant HL56143. Asterisk indicates corresponding author.

J.-Z. Tsai, H. Cao and Y. B. Choy are with the Department of Electrical and Computer Engineering, University of Wisconsin, Madison, WI 53706 USA.

J. A. Will is with the Department of Animal Health and Biomedical Sciences, University of Wisconsin, Madison, WI 53706 USA.

S. Hubbard-Van Stelle is with the Research Animal Resources Center, University of Wisconsin, Madison, WI 53705 USA.

S. Tungjitkusolmun is with the Department of Electronics Engineering, Faculty of Engineering, and the Research Center for Communications and Information Technology, King Mongkut's Institute of Technology Ladkrabang, Ladkrabang, Bangkok 10520, Thailand.

D. Haemmerich is with the Department of Biomedical Engineering, University of Wisconsin, Madison, WI 53706 USA.

V. R. Vorperian is with the University of Wisconsin Hospital and Clinics, Madison, WI 53792 USA.

*J. G. Webster is with the Department of Biomedical Engineering, University of Wisconsin, 1410 Engineering Drive, Madison, WI 53706 USA (e-mail: webster@engr.wisc.edu).

Publisher Item Identifier S 0018-9294(02)03995-2.

tance measurement. The voltage difference was sensed by a differential amplifier and then detected with phase-sensitive detection for the impedance measurement. Rigaud *et al.* [5] measured resistivity of sheep's muscle, liver, lung, spleen, and intestine in a four-electrode cell *in-vitro* from 100 Hz to 10 MHz with a Solartron 1260 impedance/gain-phase analyzer. They used the two differential amplifiers in the Solartron 1260 to measure the voltage difference and the current magnitude, respectively. Bragós *et al.* [6] measured swine myocardial resistivity *in-vivo* from 1 kHz to 1 MHz with a four-terminal plunge probe with the left anterior descending coronary artery occluded. They used an HP 4192A impedance analyzer to supply the current and to measure the current magnitude and the output voltage of a differential amplifier, which detected the voltage difference between the two voltage electrodes. Blad and Baldetorp [7] measured complex impedance of excised normal liver tissue and tumor tissue *ex-vivo* from 1.5 kHz to 700 kHz in a cylindrical chamber with four stainless-steel needles penetrating the measured tissue as the current and voltage electrodes. They used two current generators controlled by a sine wave generator. The voltage difference between the voltage electrodes was detected by a differential amplifier with two input buffers. They used two synchronous demodulators, two low-pass filters, and two digital voltmeters to measure the real and imaginary parts of the tissue impedance.

Several researchers have analyzed the error of the four-terminal measurement. Swanson and Webster [8] analyzed the errors in four-electrode impedance plethysmography due to inadequate instrumentation, improper electrode application, and physiological changes. Ackmann [3] evaluated the phase error of four-terminal measurement by experimentally manipulating the cable length and extra resistors to emulate the imbalance between the two voltage electrodes in the cable stray capacitance and the electrode-tissue interface impedance. The result was consistent with his computer simulation of an equivalent circuit model. He further measured the phase error of the lock-in amplifier, the current source, and the preamplifiers to obtain a phase calibration for the overall system. Riu *et al.* [9] used an equivalent circuit of a resistivity measurement system to analyze the requirements for limiting the magnitude of the coupling capacitance, common-mode voltage, and the voltage-measuring circuit's input impedance on the system design to attain a measurement error below 1%. Boone and Holder [10] studied the problem of attaining a high-precision electrical impedance tomograph (EIT) due to errors caused by common-mode voltage, electrode-tissue interface impedance, input impedance of the differential amplifiers, and output impedance of current sources. Al-Hatib [11] derived analytical formulas using an equivalent circuit of the patient-instrument connection for a four-terminal measurement configuration to describe the errors in the measured bioimpedance and in the overall common-mode rejection ratio (CMRR) induced by the cable capacitance in combination with the skin-electrode impedance and the bioimpedance to be measured. He further constructed an experimental circuit to demonstrate the error caused by the stray capacitance of various cable types and different values of bioimpedance and to compare the performances of a single-ended version and a symmetrical version of the current source. Scharfetter *et al.* [12] modeled with the PSpice program a whole body or segmental

bioimpedance spectroscopy system including the stray capacitance between cables, electrode leads, different body segments and earth, and signal ground and earth. They conducted simulation from 5 kHz to 1 MHz and found the latter two types of stray capacitance cause a significant spurious dispersion in the measured impedance spectra at frequencies higher than 500 kHz.

We have not found literature that leads to the evaluation or estimation of the overall error in the measured resistivity. In this study, we utilize a typical four-terminal resistivity measurement system as an example to demonstrate a systematic method for analyzing the measurement error of tissue resistivity.

II. THEORY

We have described our system and procedure for measuring tissue resistivity [13]. In this error analysis paper, we use the same equations as in that paper except that we will add error terms wherever appropriate.

Our measurement system is shown in [13, Fig. 1]. During a frequency sweep, the computer calculates the tissue resistivity at each frequency by

$$(\rho_r + \varepsilon_r) = \left(\frac{V_1}{V_2} \right) (K_o + \varepsilon_o)(K_c + \varepsilon_c)(K_w + \varepsilon_w)(K_p + \varepsilon_p). \quad (2)$$

In (2), $(\rho_r + \varepsilon_r)$ is the measured tissue resistivity with ρ_r the real tissue resistivity and ε_r the measurement error.

V_1 and V_2 are the output voltage values of channel 1 and channel 2, respectively, of the digital oscilloscope. $(K_o + \varepsilon_o)$ is the oscilloscope constant defined as $(V_v/V_i)/(V_1/V_2)$, the inverse response of the oscilloscope when measuring a voltage ratio, where V_v is the output voltage of the differential amplifier and V_i the current-to-voltage converter, respectively.

The ideal oscilloscope constant K_o equals one and the oscilloscope error ε_o accounts for the difference between the two channels of the digital oscilloscope mostly due to the quantization error.

$(K_c + \varepsilon_c)$ is the circuit constant defined as $(V_c/I_c)/(V_v/V_i)$, the inverse response of the tissue resistance-detecting circuit, where V_c is the input voltage of the differential amplifier and I_c the input current of the current-to-voltage converter. The ideal circuit constant K_c equals the ratio of the gain of the current-to-voltage converter divided by that of the differential amplifier. The circuit error ε_c is due to circuitry nonidealities, such as insufficient CMRR of the differential amplifier, finite gain of operational amplifiers in the circuits, and leakage current.

$(K_w + \varepsilon_w)$ is the wire constant defined as $(V_e/I_e)/(V_c/I_c)$, where (V_e/I_e) is the real apparent resistance of measuring the tissue with the resistivity probe and (V_c/I_c) is the apparent resistance sensed by the tissue resistance-detecting circuit. The ideal wire constant K_w is 1 and the wire error ε_w accounts for the loading effect of the stray capacitance on the signal wires between the electrodes and the circuit in series with the electrode-tissue interface impedance.

$(K_p + \varepsilon_p)$ is the measured probe constant. It contains an error term ε_p due to the inaccuracy in measuring the probe constant. The real probe constant K_p equals the ratio of the real tissue resistivity ρ_r divided by the real apparent resistance (V_e/I_e) , i.e., the inverse response of the resistivity probe, where V_e is the

voltage difference between the voltage electrodes and I_e is the current flowing through the current electrodes.

Equation (2) means that we obtain the tissue resistivity by multiplying the output ratio of the oscilloscope with the inverse responses of the oscilloscope, the circuits, the wires, and the resistivity probe. $(V_1/V_2)(K_o + \varepsilon_o)(K_c + \varepsilon_c)(K_w + \varepsilon_w)$ in (2) is equivalent to the apparent resistance in (1). Note that, in practical measurement, it is usually not necessary to measure each of the four constants separately. In our measurement, we combine the oscilloscope constant and the circuit constant into an oscilloscope-circuit constant $(K_{o-c} + \varepsilon_{o-c})$ and the wire constant and the probe constant into a wire-probe constant $(K_{w-p} + \varepsilon_{w-p})$. We re-express the equation for the measured tissue resistivity as

$$(\rho_r + \varepsilon_r) = \left(\frac{V_1}{V_2} \right) (K_{o-c} + \varepsilon_{o-c})(K_{w-p} + \varepsilon_{w-p}). \quad (3)$$

Our procedure of tissue resistivity measurement includes several steps. The following describes and formulates the error sources in each step. Note that, in the following, the subscript next to a parenthesis represents the step number in which the quantity inside the parenthesis is measured or is pertinent to the configuration used.

In *Step 1*, the measurement of the oscilloscope-circuit constant, the practical value of the oscilloscope-circuit constant calculated by the computer can be expressed as

$$(K_{o-c} + \varepsilon_{o-c})_1 = \frac{(R_f + \varepsilon_f)_1}{\left(\frac{V_1}{V_2} \right)_1} \quad (4)$$

where $(R_f + \varepsilon_f)_1$ is the resistance of the reference resistor measured with a multimeter. The error term ε_f is due to the accuracy limit of the multimeter. The exact value of R_f is unknown and the measured value $(R_f + \varepsilon_f)_1$ is used in the calculation of the oscilloscope-circuit constant. The measured value $(V_1/V_2)_1$ contains errors induced by the oscilloscope and the tissue resistance-detecting circuit. The exact value of the oscilloscope-circuit constant K_{o-c} is also unknown and the value $(K_{o-c} + \varepsilon_{o-c})_1$ measured in this step will be used in the calculation in the subsequent steps.

In *Step 2*, the measurement of saline resistivity, the measured value of the saline resistivity is

$$(\rho_s + \varepsilon_s)_2 = \left(\frac{V_1}{V_2} \right)_2 (K_{o-c} + \varepsilon_{o-c})_1 \left(\frac{A}{d} \right) (K_{A/d} + \varepsilon_{A/d})_2 \quad (5)$$

where $(A/d)(K_{A/d} + \varepsilon_{A/d})_2$ is the value of the wire-probe constant of the syringe tube, where A is the inner cross-sectional area of the syringe tube and d is the voltage electrode distance. The error term $\varepsilon_{A/d}$ is due to the inaccuracy of measuring A and d with a ruler or a caliper. The wire error at this step is less than 0.1% with 15 cm short wires between the electrodes and the circuit, 3 cm distance between the voltage electrodes, and 1 cm distance between a current electrode and its adjacent voltage electrode.

We use the oscilloscope-circuit constant $(K_{o-c} + \varepsilon_{o-c})_1$ measured in *Step 1* in this equation since we used the same circuit and the same oscilloscope in all steps.

In *Step 3*, the measurement of the wire-probe constant, the computer calculated the wire-probe constant $(K_{w-p} + \varepsilon_{w-p})_3$ as $(\rho_s + \varepsilon_s)_2 / [(V_1/V_2)_3 (K_{o-c} + \varepsilon_{o-c})_1]$ according to (2). However, we noticed that the temperature in a laboratory could be different from location to location and from time to time, and the heat emitted from the instruments could heat up the ambient temperature of the measurement site by more than 1 °C. Hence, the real value of the measured wire-probe constant is

$$(K_{w-p} + \varepsilon_{w-p})_3 = \frac{(\rho_s + \varepsilon_s)_2 (K_T + \varepsilon_T)_3}{\left(\left(\frac{V_1}{V_2} \right)_3 (K_{o-c} + \varepsilon_{o-c})_1 \right)} \quad (6)$$

where $(K_T + \varepsilon_T)_3$ represents the change of saline resistivity due to the change of the temperature in the saline solution from *Step 2* to *Step 3*, and K_T equals one. Suppose that T_2 is the saline temperature at *Step 2* and T_3 at *Step 3*, respectively, and k_s is the temperature coefficient of the saline resistivity, then $(K_T + \varepsilon_T)_3$ equals $(1 + k_s)^{(T_3 - T_2)}$. In a preliminary experiment, we measured the resistivity of saline solutions of various salt concentrations ranging from 0.1% to 1.1% at temperatures from 20 °C to 40 °C. We found that the saline resistivity decreased by 2% as the temperature increased by 1 °C. Hence, $k_s = -2\%$.

We minimized the temperature error by measuring the saline temperatures T_2 and T_3 at *Step 2* and *Step 3*, respectively, with a thermistor and by dividing the measured wire-probe constant by the temperature constant $(K_T + \varepsilon_T)_3$.

In an *in-vivo* animal experiment for myocardial resistivity measurement, such as the one described in [13], there were motion artifact [15] and electrical interference coming from the measured animal, the equipment, such as the ventilator, and the power lines running through the walls around the laboratory room. We use a noise constant $(K_n + \varepsilon_n)_3$, to represent the effect of the noise. The ideal noise constant K_n is 1 and the noise error ε_n represents the error caused by the motion artifact and the electrical interference in the *in-vivo* measurement. The noise constant is implicit in the expression of $(V_1/V_2)_3$ as $(K_n + \varepsilon_n)_3 (V_e/I_e)_3 / (K_{o-c} + \varepsilon_{o-c})_3$.

In *Step 4*, the measurement of the tissue resistivity, according to (2), the computer calculated the tissue resistivity as the voltage ratio output of the digital oscilloscope multiplied by the oscilloscope-circuit constant obtained in *Step 1* and the wire-probe constant obtained in *Step 3*. However, because the wire-probe constant could possibly change in this step, the resistivity obtained with the computer calculation is

$$(\rho_r + \varepsilon_r)_4 = \left(\frac{V_1}{V_2} \right)_4 (K_{o-c} + \varepsilon_{o-c})_1 (K_{w-p} + \varepsilon_{w-p})_3 \times (K_g + \varepsilon_g)_4 (K_i + \varepsilon_i)_4 (K_e + \varepsilon_e)_4 \quad (7)$$

where $(K_g + \varepsilon_g)_4$ is called the interpolation constant, $(K_i + \varepsilon_i)_4$, the current constant, and $(K_e + \varepsilon_e)_4$ the electrode constant, with all their ideal values K_g , K_i , and K_e being 1. The interpolation error ε_g represents the error of estimating the wire-probe constant for a measurement from a set of wire-probe constants measured by calibrating the plunge probe in each of a set of saline solutions with various resistivity values. The current error ε_i represents the deviation of the wire-probe constant due to the difference of the current magnitude during tissue resistivity

measurement and that during probe calibration. It arose due to the fact that the interface impedance between the electrode and the tissue or the saline solution changes the distribution of the current density flowing through the interface [14], [15]. The electrode error ε_e accounts for the change of the wire–probe constant caused by the action of inserting the electrodes into the tissue, which may change the electrical property of the electrode surface or alter the electrode spacing or alignment.

Just as in Step 3, there was also *in-vivo* motion artifact and electrical interference in this step. The noise constant $(K_n + \varepsilon_n)_4$ is implicit in the measured voltage ratio $(V_1/V_2)_4$, i.e., $(V_1/V_2)_4 = (K_n + \varepsilon_n)_4(V_e/I_e)_4/(K_{o-c} + \varepsilon_{o-c})_4$.

By substituting the detailed expression for $(K_{w-p} + \varepsilon_{w-p})_3$ in (7) and substituting $(V_e/I_e)_2/(K_{o-c} + \varepsilon_{o-c})_2$ for $(V_1/V_2)_2$ and $(K_n + \varepsilon_n)_j(V_e/I_e)_j/(K_{o-c} + \varepsilon_{o-c})_j$ for $(V_1/V_2)_j$, $j = 3$ to 4, based on the assumption that $(V_c/I_c) = (V_e/I_e)$ in all steps because of using short signal wires, we obtain

$$\begin{aligned} (\rho_r + \varepsilon_r)_4 = & \left[\left(\frac{V_1}{I_e} \right)_4 \right] \left(\frac{V_1}{I_e} \right)_2 (K_{oo-c-n} + \varepsilon_{oo-c-n}) \\ & \times \left(\frac{A}{d} \right) (K_{A/d} + \varepsilon_{A/d})_2 (K_T + \varepsilon_T)_3 \\ & \times (K_g + \varepsilon_g)_4 (K_i + \varepsilon_i)_4 (K_e + \varepsilon_e)_4 \end{aligned} \quad (8)$$

where $(K_{oo-c-n} + \varepsilon_{oo-c-n})$ is called the overall oscilloscope–circuit–noise constant and is defined as $[(K_{o-c} + \varepsilon_{o-c})_1(K_{o-c} + \varepsilon_{o-c})_3(K_n + \varepsilon_n)_4]/[(K_{o-c} + \varepsilon_{o-c})_2(K_{o-c} + \varepsilon_{o-c})_4(K_n + \varepsilon_n)_3]$. The reason for combining the oscilloscope–circuit constants and the noise constants is because of the difficulty of measuring them separately [see (12)]. Note that $(K_{o-c} + \varepsilon_{o-c})_1$ is a known value that has been measured in *Step 1* while $(K_{o-c} + \varepsilon_{o-c})_j$, $j = 2$ to 4, and $(K_n + \varepsilon_n)_j$, $j = 3$ to 4, are implicit values contained in the measured $(V_1/V_2)_j$, $j = 2$ to 4. The values of ε_{o-c} in the $(K_{o-c} + \varepsilon_{o-c})_j$ terms are different because they are obtained from distinct measurements.

According to (8), we express the statistics of the overall error of the measured tissue resistivity $(\rho_r + \varepsilon_r)_4$ as [16]

$$\begin{aligned} \frac{\varepsilon m_r}{\rho_r} = & \left[\frac{(K_{oo-c-n} + \varepsilon m_{oo-c-n})}{K_{oo-c-n}} \right] \left[\frac{(K_{A/d} + \varepsilon m_{A/d})_2}{K_{A/d}} \right] \\ & \times \left[\frac{(K_T + \varepsilon m_T)_3}{K_T} \right] \left[\frac{(K_g + \varepsilon m_g)_4}{K_g} \right] \\ & \times \left[\frac{(K_i + \varepsilon m_i)_4}{K_i} \right] \left[\frac{(K_e + \varepsilon m_e)_4}{K_e} \right] - 1 \end{aligned} \quad (9)$$

$$\begin{aligned} \frac{\varepsilon s_r}{\rho_r} = & \left[\left(\frac{\varepsilon s_{oo-c-n}}{K_{oo-c-n}} \right)^2 + \left(\frac{\varepsilon s_{A/d}}{K_{A/d}} \right)_2^2 + \left(\frac{\varepsilon s_T}{K_T} \right)_3^2 \right. \\ & \left. + \left(\frac{\varepsilon s_g}{K_g} \right)_4^2 + \left(\frac{\varepsilon s_i}{K_i} \right)_4^2 + \left(\frac{\varepsilon s_e}{K_e} \right)_4^2 \right]^{1/2} \end{aligned} \quad (10)$$

where εm_r , εm_{oo-c-n} , $\varepsilon m_{A/d}$, εm_g , εm_i , and εm_e are the mean values and εs_r , εs_{oo-c-n} , $\varepsilon s_{A/d}$, εs_g , εs_i , and εs_e are the standard deviations of the error terms ε_r , ε_{oo-c-n} , $\varepsilon_{A/d}$, ε_g , ε_i , and ε_e , respectively.

III. METHODS AND RESULTS

In order to evaluate the error of the measured tissue resistivity with (9) and (10), we performed a series of experiments to measure the individual error terms separately at 1 Hz, 10 Hz, 100 Hz, 1 kHz, 10 kHz, 100 kHz, 500 kHz, and 1 MHz.

To evaluate the statistics of the overall oscilloscope–circuit–noise constant $(K_{oo-c-n} + \varepsilon_{oo-c-n})$, we first measured the individual oscilloscope–circuit constants $(K_{o-c} + \varepsilon_{o-c})$ with reference resistors of nominal resistance 50, 100, 150, 200, and 250 Ω , which encompassed possible apparent resistance when measuring tissue resistivity. We measured the reference resistance with an HP 34401A multimeter. We added two other resistors to the two ends of each reference resistor to form a series combination of 1:3:1 resistance ratio. For each reference resistor we took eight measurements of the oscilloscope–circuit constant $(K_{o-c} + \varepsilon_{o-c})$, which was calculated as $(R_f + \varepsilon_f)/(V_1/V_2)$. Fig. 1(a) shows the 40 measured oscilloscope–circuit constants along with their mean and standard deviation.

Next, we measured the noise constant in an *in-vivo* condition. When an open-chest pig was alive, we put a cup of saline on top of the beating heart and immersed the plunge probe in the saline. We assumed that the noise from the pig, the ventilator, and the wall has the same effect on the measuring signals as that when we inserted the plunge electrodes in the pig’s myocardium. The computer accessed the noise-contaminated voltage ratio V_1/V_2 from the digital oscilloscope. We designated this step as *Step 5*.

After the pig died and the heart stopped beating, we turned off the ventilator and measured the voltage ratio V_1/V_2 with the plunge probe immersed in the saline solution and with the same voltage at the output of the function generator as that in the previous step. At this time, the waveform of V_v and V_i looked clean. There was little *in-vivo* noise in the measured signal and, hence, the noise error ε_n was virtually zero. We accessed the voltage ratio with a 401-time averaging and, hence, the oscilloscope–circuit error ε_{o-c} was divided by 20 and could be neglected. We call this *Step 6*.

Assuming negligible wire error, i.e., assuming $(V_c/I_c)_j = (V_e/I_e)_j$, $j = 5$ or 6, the ratio of the two measured voltage ratios will be

$$\frac{\left(\frac{V_1}{V_2} \right)_5}{\left(\frac{V_1}{V_2} \right)_6} = \frac{\left\{ \left[\frac{(V_e/I_e)_5}{(K_{o-c} + \varepsilon_{o-c})_5} \right] (K_n + \varepsilon_n)_5 \right\}}{\left\{ \left[\frac{(V_e/I_e)_6}{(K_{o-c} + \varepsilon_{o-c})_6} \right] (K_n)_6 \right\}}. \quad (11)$$

Because $(V_e/I_e)_5 = (V_e/I_e)_6$ and $K_n = 1$, (11) can be reduced to

$$\frac{\left(\frac{V_1}{V_2} \right)_5}{\left(\frac{V_1}{V_2} \right)_6} = \frac{(K_{o-c})_6 (K_n + \varepsilon_n)_5}{(K_{o-c} + \varepsilon_{o-c})_5}. \quad (12)$$

In summary, by conducting *Step 5* and *Step 6*, we obtained a quantity that characterized the combined statistic of the interference noise ε_n and the oscilloscope–circuit error ε_{o-c} at *Step 5*. Fig. 1(b) shows 152 samples of $(K_{o-c})_6(K_n + \varepsilon_n)_5/(K_{o-c} + \varepsilon_{o-c})_5$ along with their mean and standard deviation.

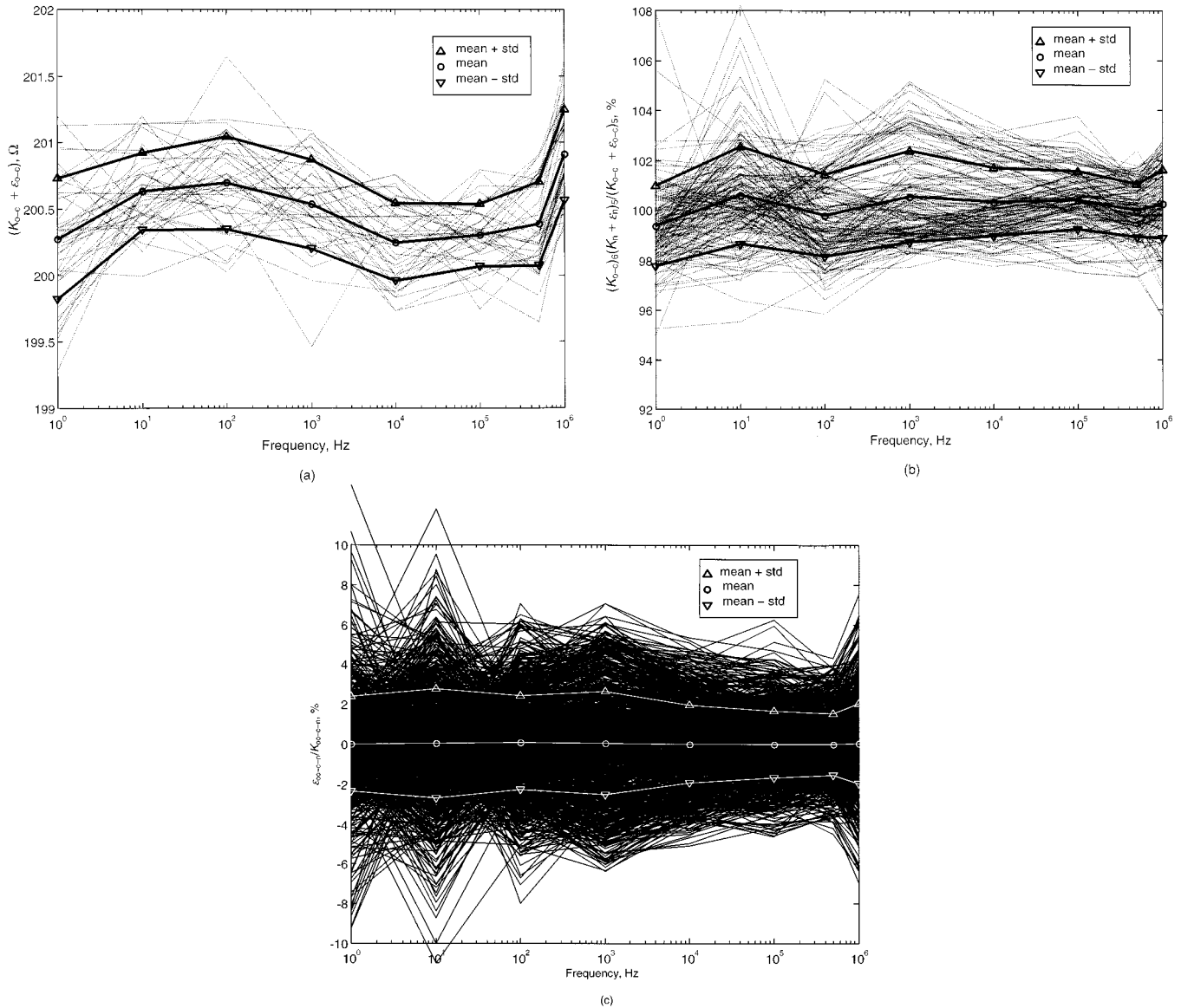


Fig. 1. (a) Forty measured samples of the oscilloscope–circuit constant $(K_{o-c} + \epsilon_{o-c})_2$ and their mean and (mean \pm standard deviation). (b) One-hundred-fifty-two measured samples of $(K_{o-c})_6(K_n + \epsilon_n)_3 / (K_{o-c} + \epsilon_{o-c})_5$ along with their mean and (mean \pm standard deviation). The measured results were used to represent the statistic of $(K_n + \epsilon_n)_3 / (K_{o-c} + \epsilon_{o-c})_3$ and $(K_n + \epsilon_n)_4 / (K_{o-c} + \epsilon_{o-c})_4$ in simulating the statistic of the overall oscilloscope–circuit–noise constant $(K_{oo-c-n} + \epsilon_{oo-c-n})$, which is defined as $[(K_{o-c} + \epsilon_{o-c})_1(K_{o-c} + \epsilon_{o-c})_3(K_n + \epsilon_n)_4] / [(K_{o-c} + \epsilon_{o-c})_2(K_{o-c} + \epsilon_{o-c})_4(K_n + \epsilon_n)_3]$. (c) One thousand simulated samples of the overall oscilloscope–circuit–noise error, $\epsilon_{oo-c-n} / K_{oo-c-n}$, and their mean and (mean \pm standard deviation).

To simulate the statistic of the overall oscilloscope–circuit–noise constant $(K_{oo-c-n} + \epsilon_{oo-c-n})$, we randomly select two from the measured oscilloscope–circuit constants shown in Fig. 1(a) and substitute them for the $(K_{o-c} + \epsilon_{o-c})_1$ and $(K_{o-c} + \epsilon_{o-c})_2$ terms in the expression of $(K_{oo-c-n} + \epsilon_{oo-c-n})$, i.e., $[(K_{o-c} + \epsilon_{o-c})_1 / (K_{o-c} + \epsilon_{o-c})_2][(K_{o-c} + \epsilon_{o-c})_3 / (K_n + \epsilon_n)_3][(K_n + \epsilon_n)_4 / (K_{o-c} + \epsilon_{o-c})_4]$. We assume that $(K_n + \epsilon_n)_3 / (K_{o-c} + \epsilon_{o-c})_3$ and $(K_n + \epsilon_n)_4 / (K_{o-c} + \epsilon_{o-c})_4$ have the same statistics as $(K_n + \epsilon_n)_5 / (K_{o-c} + \epsilon_{o-c})_5$. Hence, we randomly select two samples from the results shown in Fig. 1(b) and substitute them for $(K_n + \epsilon_n)_3 / (K_{o-c} + \epsilon_{o-c})_3$ and $(K_n + \epsilon_n)_4 / (K_{o-c} + \epsilon_{o-c})_4$ to calculate $(K_{oo-c-n} + \epsilon_{oo-c-n})$. Fig. 1(c) shows 1000 samples of the overall oscilloscope–circuit–noise constant generated this way. Fig. 2(a) shows the mean and standard deviation of $\epsilon_{oo-c-n} / K_{oo-c-n}$. Table I also shows the standard deviation.

The variation in the measured oscilloscope–circuit constant $(K_{o-c} + \epsilon_{o-c})_1$ is primarily due to the quantization error of the digital oscilloscope. The HP54600B Digital Oscilloscope provides 8-bit resolution with $\pm 1.9\%$ accuracy as described in its User and Service Guide. To measure the variation of the oscilloscope constant, we connected the probes of the two channels of the oscilloscope together to the output of the function generator and measured the voltage ratio (V_1/V_2) , which equals the value of $(K_o + \epsilon_o)$ in this configuration. We used various output amplitudes of the function generator and various vertical scales of the digital oscilloscope. We found that the variation of the measured oscilloscope constant is commensurate with that of the oscilloscope–circuit constant.

For the error $\epsilon_{A/d}$ of measuring the dimension of the syringe tube used to measure the saline resistivity in Step 2, we used a caliper with 0.01-mm resolution to measure the inner diameter

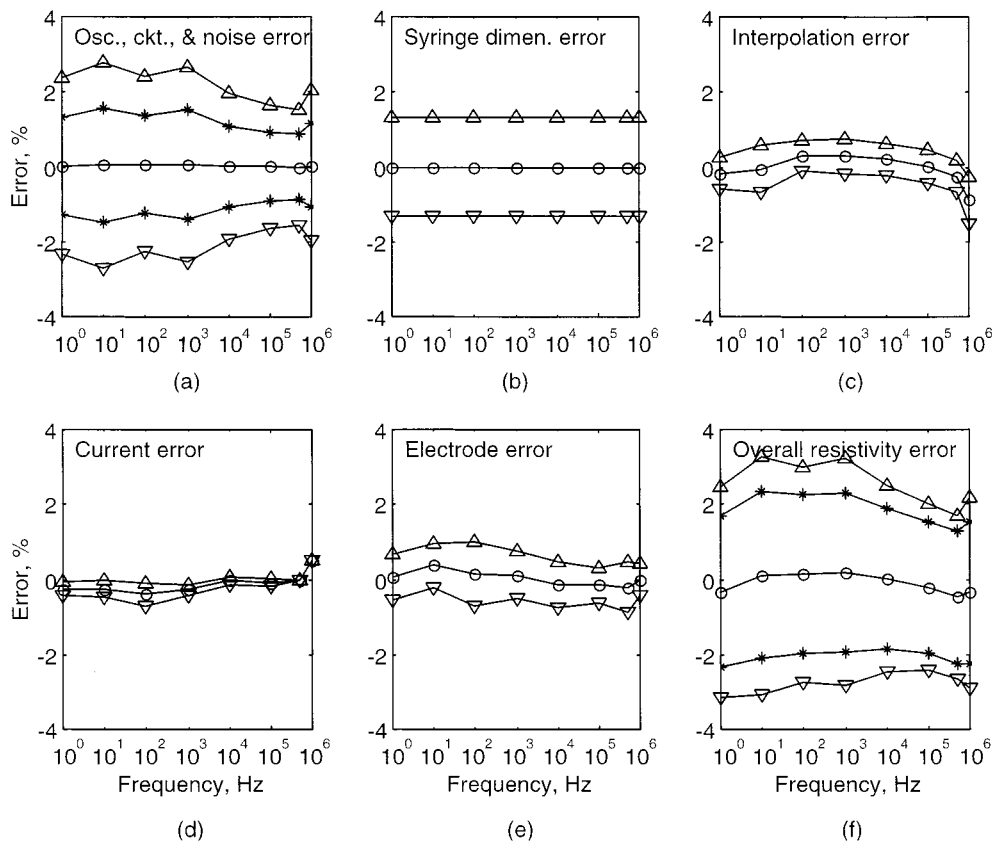


Fig. 2. The individual and overall errors of the measured myocardial resistivity. In (a) and (f), the asterisks represent the errors in the scenario of our *in-vivo* measurement, where we averaged 100 repeated measurements in *Step 1* and averaged ten repeated measurements in *Step 2* and in *Step 3*. The triangular symbols represent the errors in measurements without averaging. (a) $\varepsilon_{m_{oo-cn}}/K_{oo-cn}$ and $(\varepsilon_{m_{oo-cn}} \pm \varepsilon_{s_{oo-cn}})/K_{oo-cn}$, (b) $\varepsilon_{m_{A/d}}/K_{A/d}$ and $(\varepsilon_{m_{A/d}} \pm \varepsilon_{s_{A/d}})/K_{A/d}$, (c) ε_{m_g}/K_g and $(\varepsilon_{m_g} \pm \varepsilon_{s_g})/K_g$, (d) ε_{m_i}/K_i and $(\varepsilon_{m_i} \pm \varepsilon_{s_i})/K_i$, (e) ε_{m_e}/K_e and $(\varepsilon_{m_e} \pm \varepsilon_{s_e})/K_e$, and (f) ε_{m_r}/ρ_r and $(\varepsilon_{m_r} \pm \varepsilon_{s_r})/\rho_r$.

TABLE I
ERROR STATISTICS OF THE MEASURED TISSUE RESISTIVITY. (STANDARD DEVIATION, IN PERCENTILE)

Frequency (Hz)	1	10	100	1 k	10 k	100 k	500 k	1 M	Average
$\varepsilon_{m_{oo-cn}}/K_{oo-cn}$ (Note 1)	± 2.37	± 2.73	± 2.34	± 2.60	± 1.95	± 1.66	± 1.54	± 2.01	± 2.15
$\varepsilon_{m_{oo-cn}}/K_{oo-cn}$ (Note 2)	± 1.31	± 1.52	± 1.30	± 1.44	± 1.08	± 0.92	± 0.86	± 1.12	± 1.19
$\varepsilon_{A/d}/K_{A/d}$	± 1.32	± 1.32	± 1.32	± 1.32	± 1.32	± 1.32	± 1.32	± 1.32	± 1.32
ε_T/K_T (Note 3)	—	—	—	—	—	—	—	—	—
ε_g/K_g	± 0.42	± 0.63	± 0.41	± 0.46	± 0.45	± 0.44	± 0.44	± 0.63	± 0.48
ε_i/K_i	± 0.18	± 0.23	± 0.29	± 0.15	± 0.11	± 0.09	± 0.01	± 0.01	± 0.14
ε_e/K_e	± 0.59	± 0.65	± 0.79	± 0.62	± 0.49	± 0.28	± 0.51	± 0.49	± 0.61
ε_i/ρ_i (Note 1)	± 2.81	± 3.17	± 2.86	± 3.02	± 2.47	± 2.22	± 2.19	± 2.53	± 2.66
ε_i/ρ_i (Note 2)	± 2.01	± 2.20	± 2.10	± 2.11	± 1.87	± 1.74	± 1.77	± 1.89	± 1.96

Note 1: Without any averaging in any step.

Note 2: With 101-time, 10-time, 10-time, and no averaging in *Step 1*, *2*, *3*, and *4*, respectively.

Note 3: The temperature error became negligible after being corrected with a $-2\%/^{\circ}\text{C}$ temperature coefficient.

of the syringe and the voltage electrodes distance 15 times. The calculated value for the standard deviation of A/d is 1.32%. We assumed the mean value of the error of measuring A/d to be zero. Fig. 2(b) shows the mean and standard deviation of $\varepsilon_{A/d}/K_{A/d}$. Table I also shows the standard deviation.

The temperature error ε_T became less than 0.2% after being minimized in *Step 3* by correcting the measured wire-probe constant with the temperature coefficient of the saline solution.

To evaluate the interpolation error ε_g , we made a first set of eight saline solutions of approximately 100, 150, 200, 250, 300, 350, 400, and 500 $\Omega \cdot \text{cm}$, which covered the practical range of *in-vivo* tissue resistivity, and we measured the set of wire-probe constants in the saline solutions, just as we normally

did in *Step 2* and *Step 3* for calibrating the resistivity probe. Then we prepared a second set of seventeen saline solutions with resistivity approximately uniformly distributed between 100 and 500 $\Omega \cdot \text{cm}$. On the one hand, we estimated the plunge probe's wire-probe constants in each of the second set of saline solutions with the same method we used in *Step 4* to estimate the wire-probe constant of the plunge probe in the tissue by interpolating the measured wire-probe constants in the first set of saline solutions. On the other hand, we repeated *Step 2* and *Step 3* to practically measure the wire-probe constants in the second set of saline solutions. Fig. 3 shows the distribution of the measured and the estimated wire-probe constants in the second set of saline solutions, as well as the wire-probe constants mea-

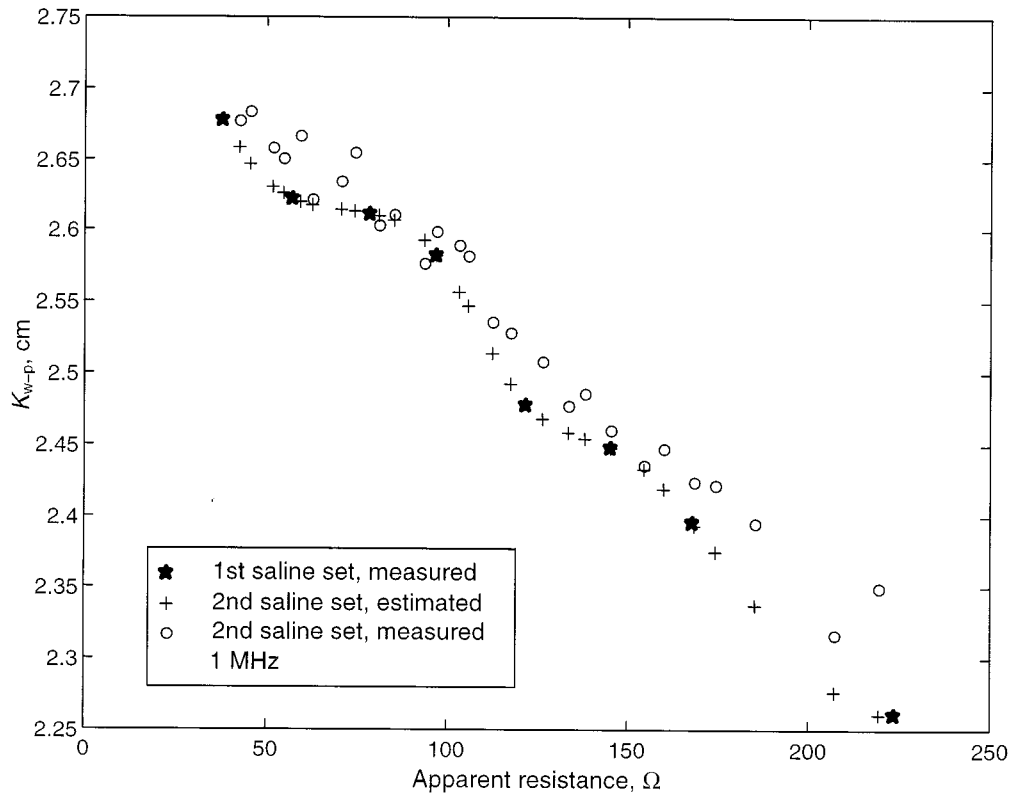


Fig. 3. The wire-probe constants K_{w-p} of the two sets of saline solution used to evaluate the interpolation error ε_g . Only the results at 1 MHz are shown here. In a practical *in-vivo* myocardial resistivity measurement, only the wire-probe constants of the first saline set are measured, and those of the myocardium (represented by the second saline set) are estimated from those of the first saline set. For the evaluation of the interpolation error, the wire-probe constants of the second saline set were also measured and the difference between the estimated and the measured wire-probe constants of the second saline set constituted the interpolation error.

measured in the first set of saline solutions, at 1 MHz. The interpolation error ε_g accounts for the difference between the estimated and the measured wire-probe constant in each of the second set of saline solutions. We further summate the interpolation error at each frequency with different weighting for different saline resistivity according to the distribution of the swine myocardial resistivity measured *in-vivo* [13]. The result is shown in Table I and Fig. 2(c).

To evaluate the current error ε_i , we first reviewed the current magnitude we used in *Step 3* and *Step 4* for our *in-vivo* measurement of swine myocardial resistivity [13] and found that the current magnitude at each frequency varied less than $\pm 20\%$ from *Step 3* to *Step 4*. We repeated *Step 3* to measure the wire-probe constants of the plunge probe in a set of saline solutions. For each saline solution, at each frequency, we measured the wire-probe constant with various current magnitudes from 80%, 84%, ..., 116%, to 120% with respect to the magnitude we normally used to calibrate the plunge probe in each of the saline solutions. We calculated the current error ε_i , as the change of the measured wire-probe constants calibrated with non-100% current magnitude with respect to that calibrated with 100% current magnitude. We further summated the current error at each frequency with different weighting for different saline resistivity according to the distribution of the swine myocardial resistivity measured *in-vivo* [13]. Fig. 4 shows the wire-probe constants measured with various current magnitudes along with their mean value and standard deviation calculated with the above-mentioned weighting. Table I and Fig. 2(d) show the statistics of the current error.

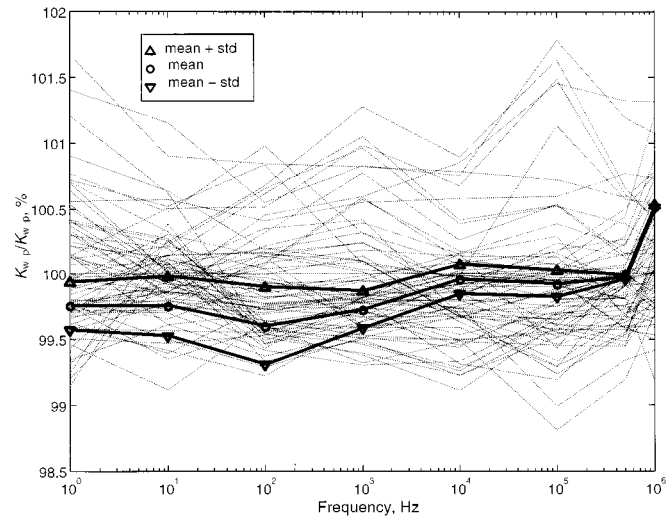


Fig. 4. The dotted lines represent the normalized wire-probe constants of the plunge probe measured in a set of saline solution with current magnitude uniformly distributed between 80% and 120% of normal values. The solid lines show the mean and (mean \pm standard deviation) of K_{w-p} calculated in accordance to the distribution of the measured swine myocardial resistivity presented in [13].

We evaluated the electrode error ε_e by observing the change of apparent resistance of a saline solution measured with the plunge probe before the first insertion into the myocardium of an open-chest pig and after each subsequent insertion. We repeated this experiment on three pigs when we were doing *in-vivo* resistivity measurement in two directions at three fixed sites of

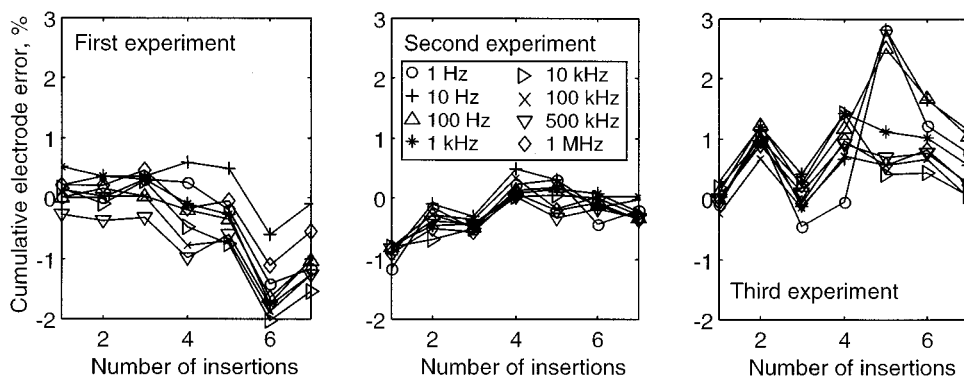


Fig. 5. Three experiments of the electrode error ε_e from insertion of the plunge probe into the myocardium of open-chest pigs' beating hearts. The apparent resistance of a saline solution was measured before the first insertion and after each insertion. The cumulative electrode error is the deviation of the apparent resistance measured after each insertion with respect to that measured before the first insertion. The electrode error shown in Table I and Fig. 5(e) is the average of the cumulative electrode error after every insertion from the three pig experiments.

each pig's left ventricle [13]. We actually had seven insertions in each of the three pigs with the extra one for re-insertion when we found the electrodes were not inserted well or the orientation of the electrode array was not in the right direction. The process included inserting the electrodes into the swine myocardium, performing resistivity measurements, pulling out the electrodes from the myocardium, rinsing them in a first saline solution, measuring the apparent resistance in a second saline solution with the same concentration as the first saline solution. We observed the difference between the apparent resistance measured in the second saline solution after the electrodes were pulled out and the apparent resistance measured before the first insertion. Fig. 5 shows the cumulative electrode error at each frequency after each insertion. We calculated the electrode error ε_e as the average of the drift of the measured apparent resistance after every insertion with respect to the preinsertion value of the three experiments. Table I and Fig. 2(e) show the statistics of ε_e/K_e from all the three *in-vivo* pig experiments.

Note that, during the measurements of ε_g and ε_e , the saline temperature could change considerably. To ensure the accuracy of the error evaluation, first we kept the saline temperature as constant as possible. Second, we measured the saline temperature with a thermistor and corrected the error caused by temperature variation with the $-2\%/^{\circ}\text{C}$ temperature coefficient.

After obtaining the statistics of all the individual errors, we estimated the overall error with (9) and (10). Table I and Fig. 2(f) show the statistics of the overall error of the measured tissue resistivity. The mean value is systematic error, we know it, and we correct for it when we report the final results [13]. Therefore, it is not shown in Table I, which shows only the standard deviation of the random error.

IV. DISCUSSION

Our system is a low-cost instrument for tissue resistivity measurement. The components used for building the differential amplifier, the current-to-voltage converter, and the temperature-measuring circuit cost less than US \$20. The year 2000 list prices of the HP54600B digital oscilloscope, HP54659B Measurement/storage module, and the HP33120A function generator are US \$2,550, US \$495, and US \$1,795, respectively. Instruments of compatible functions are readily available in most

laboratories as well as the personal computer and the LabVIEW tools. In contrast, the HP4192A impedance analyzer used by Bragós [6] costs US \$25,500, the PAR 5204 lock-in amplifier and PAR 5202 lock-in amplifier used by Ackmann [3] costs US \$10,000, the Solartron 1260 impedance analyzer used by Rigaud [5] costs US \$25,500.

It is possible to reduce the overall error in the measured resistivity by reducing individual errors.

N -time averaging of a repeated uncorrelated measurements divides the standard deviation of measurement result by a factor of $(N - 1)^{1/2}$ [16]. The digital oscilloscope provides an averaging function to reduce the quantization error. However, consistent triggering for averaging is not easy at low frequencies. We programmed our LabVIEW virtual instrument to fulfill the averaging function so that we can average even at low frequencies such as 1 Hz. In our *in-vivo* measurement, where we averaged 101 repeated measurements in *Steps 1* and ten repeated measurements in *Steps 2* and *3*, the standard deviation of ε_{osc} is theoretically divided by a factor of 1.8. The price paid is large measurement time. In our system, a resistivity measurement at eight frequencies from 1 Hz to 1 MHz takes 90 s without averaging. A resistivity measurement with ten-time averaging and 101-time averaging take 150 s and 12 min, respectively. In some situations, such as a postmortem measurement, it is not appropriate to take averaging because of the fast changes in tissue resistivity.

We can reduce the oscilloscope error by using a digital oscilloscope with higher resolution such as 14-bit resolution.

In Fig. 3, the dependence of the wire-probe constant on the apparent resistance was due to the stray capacitance between the measured animal and the ground [13]. In [13], we demonstrated how the *in-vivo* calibration alleviated the error caused by this stray capacitance. However, there was still residual error, the interpolation error ε_g , because we had to obtain the wire-probe constant for calculating the tissue resistivity by interpolating the finite set of the wire-probe constants calibrated with a set of saline solutions. It is possible to reduce the interpolation error ε_g by improving the interpolation algorithm. It is also possible to further reduce the error by calibration with more saline solutions within the target resistivity range so that the interpolation is more accurate.

In [13], we controlled the output of the function generator at constant voltage. The current magnitude during *in-vivo* tissue measurement varied less than $\pm 20\%$ from that during probe calibration. The current error ε_i can be minimized by using same current magnitude for calibrating the tissue resistivity probe in *Step 3* and for measuring the tissue resistivity in *Step 4*. Nevertheless, the current error ε_i shown in Fig. 4 has been quite small compared with other errors. Further improvement might not make much sense. The constant voltage method used in [13] is good enough, although our LabVIEW virtual instrument also provides current control modes.

Our experiment showed that the change of electrode condition after successive insertions caused a larger error than the change of a single insertion. We, thus, suggest frequent calibration during multiple insertions to reduce the electrode error ε_e .

In all four steps in our measurement procedure, we used signal wires shorter than 15 cm, which were short enough so that the error caused by the stray capacitance combined with the electrode-tissue interface impedance was less than 0.1%. In case long wires are used, driven shields [17] can minimize the error from stray capacitance. We also can minimize the effect of stray capacitance by placing the buffer stage of the tissue resistance-detecting circuit close to the electrodes.

In our analysis and experiments, we have tried to include all error sources in a typical plunge probe resistivity measurement. However, depending on the situation of the measured tissue, the electrodes configuration, and the circuits and the instruments used, there are possibly other errors. For example, when measuring myocardial resistivity with the plunge probe, there will be error due to anisotropic resistivity distribution with respect to the fiber direction; the myocardial fiber direction changes transmurally about 160° from epicardial layer to endocardial layer [18]. In an *in-vivo* measurement on an open-chest pig's ventricle, we tried to minimize the influence of the fiber direction by making a myocardial flap 1 mm wide, 1 mm thick, and 15 mm long along the local fiber direction with one end still connected to the heart. We laid the flap in a four-electrode rectangular tube with the same cross-sectional area as the flap to measure the myocardial resistivity along the fiber direction. Repeated measurements showed considerable change and variation of myocardial resistivity in the rectangular tube. We speculate that ischemia caused deviation of the myocardial resistivity [6], [19], [20]. As another error source, the in-chamber blood, which has different resistivity than myocardium, can perturb the myocardial resistivity measurement if the interelectrode distance or the insertion depth of the plunge electrodes is large compared with the myocardial thickness [21]. Our *in-situ* measurements with plunge probes [13] showed that the swine myocardial resistivity at low frequencies changed considerably after the pig's heart stopped beating. The resistivity below 1 kHz could increase by 50% within 60 min and it could double after 100 min. The resistivity at 500 kHz and 1 MHz increased by less than 15% within 6 h after the pig died. The results of *in-vitro* measurements also depend on time as well as how the tissue has been treated before measurement. These time factors add to overall resistivity error when comparing tissue resistivity measured at different times.

We made several surface resistivity probes where the four electrodes were lying on the surface of an epoxy base. Repeated

measurements on myocardium or agar phantoms with these surface probes showed possibly over 10% variations of measured resistivity. We suspect the variation came from the variation of the contact between the electrodes and the measured media. Similar error could occur with the surface point probe used by Steendijk *et al.* [4] if good contact could not be ensured. Steendijk *et al.* fixed the resistivity probe on the epicardial surface of the beating heart with a flexible silicone rubber suction cup whose inner space was maintained at a slight vacuum with a pump. We repeated this measurement with our own suction cup, but found vacuum-induced bruise on the epicardium under the cup, which has an unknown effect on the myocardial resistivity. Accordingly, we recommend not using surface probes. Instead, in our *in-vivo* measurement [13], we used plunge probes to cope with the contact variation error of surface probes.

When we measured the noise constant at *Step 5*, we assumed same statistical characteristics of the noise signals measured by inserting the plunge electrodes into the myocardium and by immersing the electrodes in a saline solution contained in a metal cup on the top of the open-chest animal's heart. This assumption was based on the fact that there was no removing or adding of noise sources between the two conditions and the fact that the observed amplitude and time characteristics of the noise waveforms in the two conditions were similar. Note that this assumption is valid only when the noise remains stationary, which is a condition that cannot always be guaranteed in a clinical environment.

Our system is capable of measuring the phase angle as well as the magnitude of the tissue resistivity. However, in our *in-vivo* measurement of swine myocardial resistivity, we found that the digital oscilloscope sometimes failed to provide stable phase measurement if the interference noise became too large compared with the signal. When the phase measurement of tissue resistivity is desired in a noisy measurement situation, we suggest the use of extra circuits to filter out the noise or even the adoption of the more costly phase-sensitive detection technique used by Ackmann [3], instead of our low-cost measurement method, for more stable phase measurement. Nevertheless, similar procedures and formulas as those presented in this paper can be used to evaluate the error of the measured phase angle of the tissue resistivity.

V. CONCLUSION

We analyzed the performance of a commonly used tissue resistivity measurement configuration in terms of the measurement error of the tissue resistivity. We identified error sources and derived the analytical equation of the measurement error step by step following the tissue resistivity measurement procedure. We evaluated the error terms in the analytical equation by *in-vivo* or bench-top experiments. The total error in the measured resistivity varies depending on the accuracy of the instruments, the characteristic of the circuit, the stray capacitance of the signal wires, the temperature change during the measurement procedure, the tissue resistivity, the current magnitude during measurement, the electrode bending and surface condition of the four-terminal resistivity probe, and the stray capacitance between the measured object and ground. Our error

evaluation method remains applicable for different circuits and instruments, or different resistivity probe configurations.

REFERENCES

[1] A. van Oosterom, R. W. de Boer, and R. T. van Dam, "Intramural resistivity of cardiac tissue," *Med. Biol. Eng. Comput.*, vol. 17, no. 3, pp. 337-343, 1979.

[2] E. Zheng, S. Shao, and J. G. Webster, "Impedance of skeletal muscle from 1 Hz to 1 MHz," *IEEE Trans. Biomed. Eng.*, vol. BME-31, pp. 477-481, June 1984.

[3] J. J. Ackmann, "Complex bioelectric impedance measurement system for the frequency range from 5 Hz to 1 MHz," *Ann. Biomed. Eng.*, vol. 21, no. 2, pp. 135-146, 1993.

[4] P. Steendijk, E. T. van der Velde, and J. Baan, "Dependence of anisotropic myocardial electrical resistivity on cardiac phase and excitation frequency," *Basic Res. Cardiol.*, vol. 89, no. 5, pp. 411-426, 1994.

[5] B. Rigaud, L. Hamzaoui, M. R. Frikha, N. Chauveau, and J.-P. Morucci, "In-vitro tissue characterization and modeling using electrical impedance measurements in the 100 Hz-10 MHz frequency range," *Physiol. Meas.*, vol. 16, pp. A15-A28, 1995.

[6] R. Bragós, A. Yáñez, P. J. Riu, M. Tresánchez, M. Warren, A. Carreño, and J. Cíncas, "Espectro de la impedancia del miocardio porcino in-situ durante la isquemia. Parte I: Sistema de medida," presented at the Proc. XIV Congreso Anual de la Sociedad española de Ingeniería Biomédica, Pamplona, Spain, 1996, pp. 97-99.

[7] B. Blad and B. Baldetorp, "Impedance spectra of tumour tissue in comparison with normal tissue; a possible clinical application for electrical impedance tomography," *Physiol. Meas.*, vol. 17, no. Suppl. 4A, pp. A105-115, 1996.

[8] D. K. Swanson and J. G. Webster, "Errors in four electrode impedance plethysmography," *Med. Biol. Eng. Comput.*, vol. 21, pp. 674-680, 1983.

[9] P. J. Riu, J. Rosell, A. Lozano, and R. Pallas-Areny, "Multi-frequency static imaging in electrical impedance tomography: Part 1 instrumentation requirements," *Med. Biol. Eng. Comput.*, vol. 33, pp. 784-792, 1995.

[10] K. G. Boone and D. S. Holder, "Current approaches to analogue instrumentation design in electrical impedance tomography," *Physiol. Meas.*, vol. 17, pp. 229-247, 1996.

[11] F. Al-Hatib, "Patient-instrument connection errors in bioelectrical impedance measurement," *Physiol. Meas.*, vol. 19, pp. 285-296, 1998.

[12] H. Scharfetter, P. Hartinger, H. Hinghofer-Szalkay, and H. Hutten, "A model of artefacts produced by stray capacitance during whole body or segmental bioimpedance spectroscopy," *Physiol. Meas.*, vol. 19, pp. 247-261, 1998.

[13] J.-Z. Tsai, J. A. Will, S. H.-V. Stelle, H. Cao, S. Tungjitsulmun, Y. B. Choy, D. Haemmerich, V. R. Vorperian, and J. G. Webster, "In-vivo measurement of swine myocardial resistivity," *IEEE Trans. Biomed. Eng.*, vol. 49, pp. 472-483, May 2002.

[14] D. P. Das and J. G. Webster, "Defibrillation recovery curves for different electrode materials," *IEEE Trans. Biomed. Eng.*, vol. BME-27, pp. 230-233, Apr. 1980.

[15] M. R. Neuman, "Biopotential electrodes," in *Medical Instrumentation: Application and Design*, 3rd ed, J. G. Webster, Ed. New York: Wiley, 1998.

[16] E. O. Doebelin, *Measurement Systems: Application and Design*, 4th ed. New York: McGraw-Hill, 1990, p. 51 and 63.

[17] R. Pallás-Areny and J. G. Webster, *Sensors and Signal Conditioning*, 2nd ed. New York: Wiley, 2001.

[18] D. D. Streeter, H. M. Spotnitz, D. J. Patel, J. Ross, and E. H. Sonnenblick, "Fiber orientation in the canine left ventricle during diastole and systole," *Circ. Res.*, vol. 24, pp. 339-347, 1969.

[19] M. M. Gebhard, E. Gersing, C. J. Brockhoff, P. A. Schnabel, and H. J. Bretschneider, "Impedance spectroscopy: A method for surveillance of ischemia tolerance of the heart," *Thorac. Cardiovasc. Surg.*, vol. 35, no. 1, pp. 26-32, 1987.

[20] M. A. Fallert, M. S. Mirotznik, S. W. Downing, E. B. Savage, K. R. Foster, M. E. Josephson, and D. K. Bogen, "Myocardial electrical impedance mapping of ischemic sheep hearts and healing aneurysms," *Circulation*, vol. 87, no. 1, pp. 199-207, 1993.

[21] J.-Z. Tsai, H. Cao, S. Tungjitsulmun, E. J. Woo, V. R. Vorperian, and J. G. Webster, "Dependence of apparent resistance of four-electrode probes on insertion depth," *IEEE Trans. Biomed. Eng.*, vol. 47, pp. 41-48, Jan. 2000.

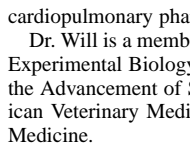


Jang-Zern Tsai was born in Chia-Yi, Taiwan, in 1961. He received the B.S.E.E. degree from National Central University, Chung-Li, Taiwan, in 1984, and the M.S.E.E. degree from National Tsing Hua University, Hsinchu, Taiwan, in 1986. In 2001, he received the Ph.D. degree in electrical and computer engineering from University of Wisconsin at Madison, doing research on myocardial resistivity measurement.



He joined the Industrial Technology Research Institute (ITRI), Hsinchu, Taiwan, as an Integrated-Circuit Applications Engineer and as a Hardware Engineer working on digital recording technology and the Accton Technology Corporation, Hsinchu, Taiwan, as a Software Engineer. He is presently a Postdoctoral Fellow at the University of California-Berkeley developing hardware for electrical impedance tomography.

James A. Will received the B.S. degree in agriculture in 1952, the M.S. degree in animal science in 1953 and the Ph.D. degree in veterinary science in 1967 from the University of Wisconsin-Madison. He received the D.V.M. degree from Kansas State University, Manhattan, in 1960.



Since 1967, he has been with the University of Wisconsin-Madison, serving as Professor and Chairman of Veterinary Science from 1974 to 1978. He has 108 reviewed publications in animal surgery, specializing in pulmonary circulation and cardiopulmonary pharmacology.

Dr. Will is a member of the American Physiological Society, the Society For Experimental Biology and Medicine, Sigma Xi, the American Association for the Advancement of Science, the American Heart Association, and the American Veterinary Medical Association. He is a Fellow of the Royal Society of Medicine.



Scott Hubbard-Van Stelle attended the University of Wisconsin-Madison from 1974-1976. He received his Associate of Applied Science degree in 1978 from the Madison Area Technical College and became a certified Veterinary Technician.

Since then, he has worked at the University of Wisconsin-Madison as a Research Specialist for 18 years and currently as a Laboratory Animal Training Coordinator.

He became a member of the American Association of Laboratory Animal Science in 1979 and was certified as a Laboratory Animal Technologist in 1993.



Hong Cao (S'97) received the B.S. and M.S. degrees in electrical engineering from Nanjing University, Nanjing, China in 1992 and 1995, respectively. He received the Ph.D. degree in electrical and computer engineering from the University of Wisconsin-Madison in 2001.

Currently, he is a Senior Software Developer with Epic System Corporation, Madison, WI, working on the enterprise electronic medical record (EMR) database system and integration of medical instruments into the EMR system. His research interests include medical instrumentation, RF catheter ablation of cardiac tissue and hepatic tumors, and medical information systems. He is contributing author to J. G. Webster (Ed.), *Minimally Invasive Medical Technology* (Bristol, UK: IOP, 2001).



Supan Tungjikusolmun (S'96-M'00) was born in Bangkok, Thailand, December 5, 1972. He received the B.S.E.E. degree from the University of Pennsylvania, Philadelphia, in 1995, and the M.S.E.E. and the Ph.D. degrees from the University of Wisconsin, Madison, in 1996, and 2000.

He is on the faculty of the Department of Electronics, Faculty of Engineering, and the Research Center for Communications and Information Technology, King Mongkut's Institute of Technology Ladkrabang (KMILT), Bangkok, Thailand. His research interests include finite-element modeling, radio-frequency cardiac ablation, and hepatic ablation.

Dr. Tungjikusolmun is a member of Tau Beta Pi, Eta Kappa Nu, and Pi Mu Epsilon.



Young Bin Choy (SM'00) was born in Seoul, Korea, on Aug 17, 1976. He received the B.S. degree in 1999 from the School of Electrical Engineering, Seoul National University, Seoul, Korea. He received the M.S.E.E degree in 2000 from the University of Wisconsin-Madison. His research was measuring the mechanical compliance of the endocardium to determine the relation between the penetration depth of the RF cardiac catheter ablation electrode and the force. He is currently a Ph.D. candidate at the University of Illinois at Urbana-Champaign.

He was an Engineer in LG Corporate Institute of Technology, Seoul, Korea, from January to June 1999.



Dieter Haemmerich (S'00) was born in Vienna, Austria, on May 22, 1971. He received the B.S.E.E. degree from the Technical University of Vienna, Vienna, Austria, in 1997 and the M.S.B.M.E. and the Ph.D. degree from the Department of Biomedical Engineering, University of Wisconsin, Madison, in 2000 and 2001, respectively.

He is currently an Assistant Scientist in the Department of Surgery, University of Wisconsin, Madison. His research interests include finite-element analysis of radio-frequency ablation and tissue

impedance measurement.



Vicken R. Vorperian received the M.D. degree in 1985 from the American University of Beirut, Beirut, Lebanon. He did a fellowship in cardiac arrhythmias and electrophysiology at the Vanderbilt University, Nashville, TN; and a fellowship in cardiac pacing and catheter ablation at the University of Michigan, Ann Arbor.

He is Clinical Associate Professor of Medicine in the Department of Medicine, University of Wisconsin-Madison and is an Electrophysiologist in the Cardiac Electrophysiology Laboratory, the University of Wisconsin Hospital, Madison. He is also a member of the Arrhythmia Consultants of Milwaukee S.C., a private practice group in cardiac arrhythmias and clinical cardiac electrophysiology.



John G. Webster (M'59-SM'69-F'86-LF'97) received the B.E.E. degree from Cornell University, Ithaca, NY, in 1953, and the M.S.E.E. and Ph.D. degrees from the University of Rochester, Rochester, NY, in 1965 and 1967, respectively.

He is Professor of Biomedical Engineering at the University of Wisconsin-Madison. In the field of medical instrumentation he teaches undergraduate and graduate courses, and does research on RF cardiac and hepatic ablation. He is editor of *Medical instrumentation: application and design, Third Edition* (New York: Wiley, 1998), *Encyclopedia of electrical and electronics engineering* (New York: Wiley, 1999), and *Minimally invasive medical technology* (Bristol, UK: IOP, 2001).

Dr. Webster is the recipient of the 2001 IEEE-EMBS Career Achievement Award.

Dr. Webster is the recipient of the 2001 IEEE-EMBS Career Achievement Award.